Geomechanics and Engineering, *Vol. 27, No. 2 (2021) 115-121*
https://doi.org/10.12989/gae.2021.27.2.115

Seismic analysis of soil-structure interaction: Experimentation and modeling

Van Quan Huynh[1a], Trung Kien Nguyen[2b] and Xuan Huy Nguyen*[2]

[1]*Campus in Ho Chi Minh city, University of Transport and Communications, Ho Chi Minh City, Vietnam*
[2]*Research and Application Center for Technology in Civil Engineering (RACE), University of Transport and Communications, Hanoi, Vietnam*

(Received June 1, 2020, Revised April 3, 2021, Accepted October 5, 2021)

Abstract. This paper presents a simplified modelling strategy to simulate the soil-foundation-structure interaction under seismic loadings. The interaction of soil and structure is modeled by a macro-element with the coupling of geometric and material non-linearities. The model consists of 4 degrees of freedom in which the superstructure is lumped as a single degree of freedom (DOF) while the soil-foundation is modeled by 3 DOFs. The dynamic equilibrium equations are solved by a Newmark time integration scheme and implemented in Matlab. To verify the numerical model, an experimental investigation based on shaking table method has been conducted in the present study. Five series of earthquake motions with maximum acceleration increased from 0.1 $\boldsymbol{m/s^2}$ to 1.4 $\boldsymbol{m/s^2}$were applied and the results of time-dependent accelerations and displacements are extracted. Based on the result comparisons, it is found that the numerical results were well validated against the experimental results.

Keywords: experimentation; macro-element; seismic loading; shaking table test; soil-structure interaction

1. Introduction

Dynamic analysis of the soil-structure interaction (SSI) is important in the field of earthquake engineering. Classical approaches based on finite element analyses have been used to analyze the SSI problem. Although the method can provide accurate results for the problem, it is expensive and complex solutions and it also consume a lot of time and efforts. Introduced in the early nineties in the framework of strip footings on sand (Nova and Montrasio 1991), the solutions based on a macro-element has been described as a practical approach that can capture the soil-structure interaction. The main idea of the model is that the soil-structure interaction domain is reduced to a point at the center of the footing with geometric and material non-linearities.

In the last decade, many studies were conducted to simulate the SSIs and to investigate their effects by using a macro-element approach (Chatzigogos *et al.* 2011, Figini *et al.* 2012, Pecker *et al.* 2014, Venanzi *et al.* 2014, Salciarini *et al.* 2016, Chai *et al.* 2017, Page *et al.* 2018, Page *et al.* 2019, Huynh *et al.* 2020, Tistel, J *et al.* 2020). Basing on a macro-element model presented in the study of Nova and Montrasio (1991), Paolucci (1997) was the first study to implement the macro-element model into dynamic seismic analysis. Cremer *et al.* (2001, 2002) developed the macro-element for purely cohesive soils, considering the plasticity of the soil and the uplift of the foundation. Paolucci *et al.* (2008) introduced a simple degradation rule of the foundation stiffness parameters, suitable to capture the rocking response and focus on the significant reduction in the foundation–soil contact area. Di Prisco *et al.* (2011), Grange *et al.* (2008, 2009) and Chatzigogos *et al.* (2009, 2011) generated macro-elements for shallow foundations with coupled plasticity and uplift mechanisms for undrained soil conditions. They are all based on the same concepts as that derived by Cremer *et al.* (2001, 2002) with simpler and easier-to-use constitutive models (Pecker *et al.* 2014). The dynamic macro-element of Figini *et al.* (2012) adopted the degradation model used by Paolucci *et al.* (2008) and the uplift model was based on work by Chatzigogos *et al.* (2009). The macro-element formulation of Millen *et al.* (2018) used the uplift model from Chatzigogos *et al.* (2009), and the plasticity formulation from Figini *et al.* (2012). Khebizi *et al.* (2018) used a "gap" element connected in a series with a non-linear link in order to form a new macro-element, the horizontal behavior of the foundation controlled by a non-linear horizontal link, the soil foundation system modelled by a rigid beam resting on a set of the vertical macro-elements according to the Winkler approach. Recently, Huynh *et al.* (2020) proposed a macro-element for simulating the seismic behavior of the soil-shallow foundation interaction. This was a 3-DOF macro-element and considered the effects of material and geometric nonlinearities on the response of foundation.

The present work is a contribution aiming to propose a macro-element model with the coupling of geometric and material non-linearities. The macro-element consists of 4 DOFs in which the superstructure is lumped as a single DOF and the system of soil-foundation is modeled by 3 DOFs. The dynamic equilibrium equations of the system

∗Corresponding author, Associate Professor
E-mail: nguyenxuanhuy@utc.edu.vn
[a] Ph.D. Student
E-mail: hvquan@utc2.edu.vn
[b]Associate Professor
E-mail: ntkien@utc.edu.vn

ISSN: 2005-307X (Print), 2092-6219 (Online)

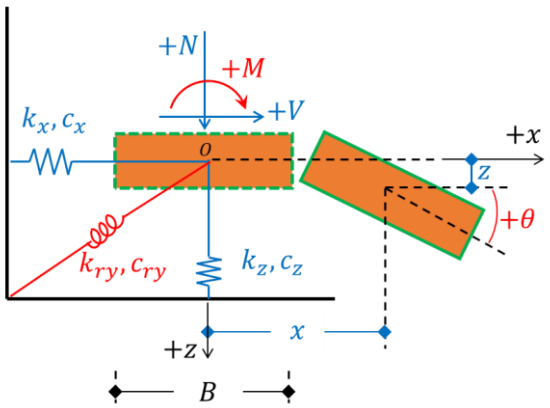

Fig. 1 Generalized forces and displacements in case of a strip (shallow) foundation

will be established in detail and solved by the well-known Newmark time integration scheme. The numerical results are compared with the experimental data which performed on shaking table tests. In the last part of paper, the Paolucci's model are also discussed and compared with the proposed macro-element model and experimentation.

2. Non-linear macro-element model

2.1 The dynamic equilibrium equations

The constitutive equations of the macro-element are written in terms of generalized forces and displacement variables (see Fig. 1) (Figini *et al.* 2012). Whereas, N, V and M are the vertical force, horizontal force and moment applied to the foundation, respectively; z and x are the vertical and horizontal displacements of the footing, θ is its rotation angle.

The dynamic equilibriums of the system in Fig. 2 can be described by the following equation:

$$\boldsymbol{M}\ddot{\boldsymbol{u}} + \boldsymbol{C}\dot{\boldsymbol{u}} + \boldsymbol{F}^S + \boldsymbol{F}^F = \boldsymbol{P} \tag{1}$$

Where

$$\boldsymbol{u} = [x_1 \quad x_0 \quad \theta \quad z]^T \tag{2}$$

$$\boldsymbol{P} = [-m_1\ddot{x}_g \quad -m_0\ddot{x}_g \quad 0 \quad -(m_0+m_1)\ddot{z}_g]^T \tag{3}$$

$$\boldsymbol{F}^F = [0 \quad V \quad M \quad N]^T \tag{4}$$

$$\boldsymbol{M} = \begin{bmatrix} m_1 & 0 & 0 & 0 \\ 0 & m_0 & 0 & 0 \\ 0 & 0 & J & 0 \\ 0 & 0 & 0 & m_1+m_0 \end{bmatrix} \tag{5}$$

$$\boldsymbol{K}^S = \begin{bmatrix} k_{1x} & -k_{1x} & -k_{1x}h & 0 \\ -k_{1x} & k_{1x} & k_{1x}h & 0 \\ -k_{1x}h & k_{1x}h & k_{1x}h^2 & 0 \\ 0 & 0 & 0 & 0 \end{bmatrix} \tag{6}$$

$$\boldsymbol{C} = \begin{bmatrix} c_{1x} & -c_{1x} & -c_{1x}h & 0 \\ -c_{1x} & c_{1x}+c_x & c_{1x}h & 0 \\ -c_{1x}h & c_{1x}h & c_{1x}h^2+c_{ry} & 0 \\ 0 & 0 & 0 & c_z \end{bmatrix} \tag{7}$$

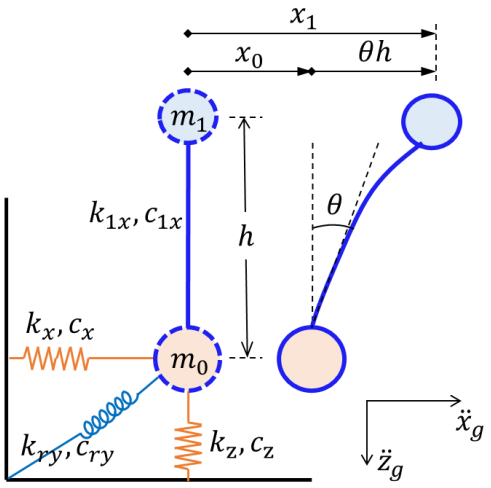

Fig. 2 4 DOFs analytical model with macro-element

where x_1 is the lateral displacement of the superstructure; x_0, z, θ are the displacements and the rocking motion of the basement (Fig. 1); $\boldsymbol{F}^F$ is the vector of soil reactions (see Fig. 1); $\boldsymbol{P}$ is the vector of base excitations; $\boldsymbol{F}^S = \boldsymbol{K}^S\boldsymbol{u}$ is the vector of the structural elastic forces, k_{1x} is the elastic stiffness of the superstructure; $\ddot{x}_g$, $\ddot{z}_g$ are the horizontal and vertical base excitations; m_1, m_0 are the effective mass of the superstructure and foundation; J is the sum of the centroid moments of inertia of the superstructure and the foundation; h is the effective height of the superstructure; c_{1x} is the damping of the superstructure; c_x, c_{ry}, c_z are the equivalent dash-pot coefficients of the soil-foundation system corresponding to the horizontal, rocking and vertical modes of vibration, respectively.

The dynamic equilibrium equations in Eq. (1) solved by well-known Newmark's time integration scheme. Denoting by the subscript n the quantities calculated at time $t = n\Delta t$, Eq. (1) can be rewritten as:

$$\begin{aligned} &\left[\frac{\boldsymbol{M}}{\beta(\Delta t)^2} + \frac{\boldsymbol{C}\gamma}{\beta\Delta t} + \boldsymbol{K}^S\right]\boldsymbol{u}_{n+1} + \boldsymbol{F}_{n+1}(\boldsymbol{u}_{n+1}) \\ &\quad = \boldsymbol{P}_{n+1} \\ &\quad + \boldsymbol{M}\left[\frac{1-2\beta}{2\beta}\ddot{\boldsymbol{u}}_n + \frac{\dot{\boldsymbol{u}}_n\Delta t + \boldsymbol{u}_n}{\beta(\Delta t)^2}\right] \\ &\quad + \boldsymbol{C}\left[\left(\frac{\gamma}{2\beta}-1\right)\ddot{\boldsymbol{u}}_n\Delta t + \left(\frac{\gamma}{\beta}-1\right)\dot{\boldsymbol{u}}_n \right. \\ &\quad \left. + \frac{\gamma}{\beta\Delta t}\boldsymbol{u}_n\right] \end{aligned} \tag{8}$$

2.2 The yield function and flow rule

The yield function and flow rule are based on the Nova and Montrasio's model:

$$f(\boldsymbol{F}) = h^2 + m^2 - v^2(1-v)^{2\xi} \tag{9}$$

where $h = V/(\mu N_{max})$, $m = M/(\psi B N_{max})$, $v = N/N_{max}$; N_{max} is the ultimate bearing capacity under

vertical central load. The shape of the plasticity bounding surface, Eq. (9), is governed through the parameters μ and ψ. From experience in laboratory experiments, μ can be evaluated as $\mu = \frac{3}{4}tan\varphi$, where φ is the soil friction angle (Figini *et al.* 2012). For the yield function parameters, ψ can be defined according to the ultimate capacity of the footing under eccentric loading; $\psi = 0.33$ according to the Meyerhof (1953), $\psi = 0.48$ according to Vesic (1975), the typical values of ψ lie within the $0.35 \div 0.5$ range; $\psi = 0.43$ was selected, that is an intermediate value (Paolucci *et al.* 2008). ξ is taken equal to 0.95 (Paolucci *et al.* 2008, Figini *et al.* 2012).

The shape of the plastic potential surface which proposed by Cremer *et al.* (2001) will be adopted (Paolucci *et al.* 2008, Figini *et al.* 2012, Millen *et al.* 2018):

$$g(\boldsymbol{F}) = \lambda^2 h^2 + \chi^2 m^2 + v^2 - 1 \tag{10}$$

where λ and χ are two non-dimensional parameters, which have to be calibrated based on experimental tests. The optimum parameters $\lambda = 4$ and $\chi = 6$ were selected (Cremer *et al.* 2001).

2.3 The stiffness matrix of macro-element

The vector of soil reactions at time step $n+1$ can be calculated by the following formula: $\boldsymbol{F}^F_{n+1} = \boldsymbol{F}^F_n + \boldsymbol{K}^F(\boldsymbol{u}_{n+1} - \boldsymbol{u}_n)$. $\boldsymbol{K}^F$ is given by Eq. (11) (Paolucci 1997, Paolucci *et al.* 2008, Chatzigogos *et al.* 2009, Figini *et al.* 2012, Millen *et al.* 2018).

$$\boldsymbol{K}^F = \begin{bmatrix} 0 & 0 & 0 & 0 \\ 0 & k_x & 0 & 0 \\ 0 & 0 & k_{ry} & 0 \\ 0 & 0 & 0 & k_z \end{bmatrix} \tag{11}$$

where k_x, k_{ry} and k_z are the foundation static impedances corresponding to the translational, rocking and vertical modes of vibration, respectively. These values depend on the foundation geometry and on the elastic parameters of the soil, which can be determined from standard formulas (Gazetas 1991).

During the strong seismic excitation, the geometric and material non-linearity changes over time (see Fig. 3) (Anastasopoulos *et al.* 2012, Paolucci *et al.* 2008). The instantaneously effective foundation width (B') can be expressed as:

$$B' = B(1 - \delta) \tag{12}$$

where B is the width of the footing, δ can be interpreted as a degradation parameter defined in the range $0 \le \delta < 1$. Initially, the value of δ is set to zero, and δ is updated throughout the seismic excitation due to accumulation of inelastic foundation tilting. The reduced foundation impedances for each vibration mode are obtained by replacing Eq. (12) into the approximate static stiffness formulas for footings (e.g., Gazetas 1991). The following degradation function has been proposed by Paolucci *et al.* (2008):

$$\delta(\theta) = \frac{\delta_1}{1 + \frac{1}{\delta_2 \theta}} \tag{13}$$

where δ_1 and δ_2 are model parameters related to the ultimate value of δ and to the degradation speed, respectively. δ_1 and δ_2 are chosen to reproduce the variation of the elastic stiffness (in particular the uplift) as a function of the cumulated plastic rotation. In the calculations, δ_1=0.75 and δ_2=5000/rad are used for all the excitations under study (Paolucci *et al.* 2008). At a specified instant of time, θ is given by Eq. (14). In Eq. (14), n and M_n are the increments of foundation rotation and overturning moment, respectively, calculated at the nth time step; k'_{ry} is the modified rocking stiffness in terms of δ.

$$\theta = \sum\nolimits_n \left| \Delta\theta - \Delta M / k'_{ry} \right| \tag{14}$$

According to Cremer *et al.* (2001), the soil behavior is assumed to be linear visco-elastic until the failure surface in Eq. (9) is reached. The plastic flow occurs when $f(\boldsymbol{F}) \ge 0$ and $df(\boldsymbol{F}) = 0$. The elastic stiffness matrix of macro-elements will be reduced by a differential value $d\boldsymbol{K}^F$, a function of the elastic stiffness matrix $\boldsymbol{K}^F$ and the derivatives of the yield and plastic potential functions (Paolucci 1997).

$$d\boldsymbol{K}^F = \boldsymbol{K}^F \left(\frac{\partial g}{\partial \boldsymbol{F}}\right) \left(\frac{\partial f}{\partial \boldsymbol{F}}\right)^T \boldsymbol{K}^F \left[\left(\frac{\partial f}{\partial \boldsymbol{F}}\right)^T \boldsymbol{K}^F \left(\frac{\partial g}{\partial \boldsymbol{F}}\right)\right]^{-1} \tag{15}$$

3. Experimental verification

3.1 Shaking table test

The experimental study has been conducted at the University of Transport and Communications, Hanoi,

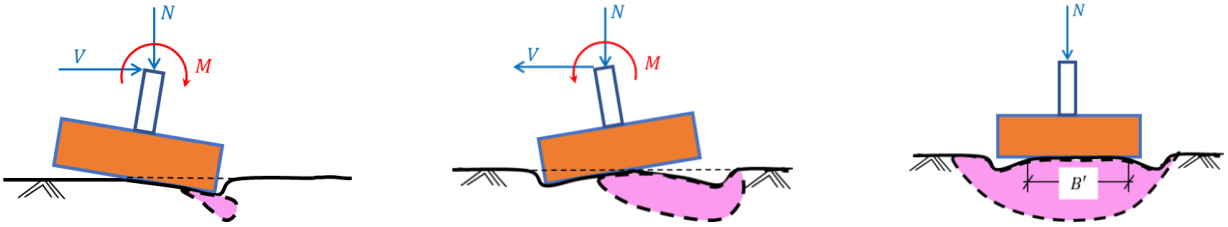

(a) Decreased contact width beneath the foundation

(b) The material non-linearity is mobilized

(c) The geometric and material non-linearity is accumulative and substantial

Fig. 3 Sketch of geometric and material non-linearity in dynamic soil-foundation interaction

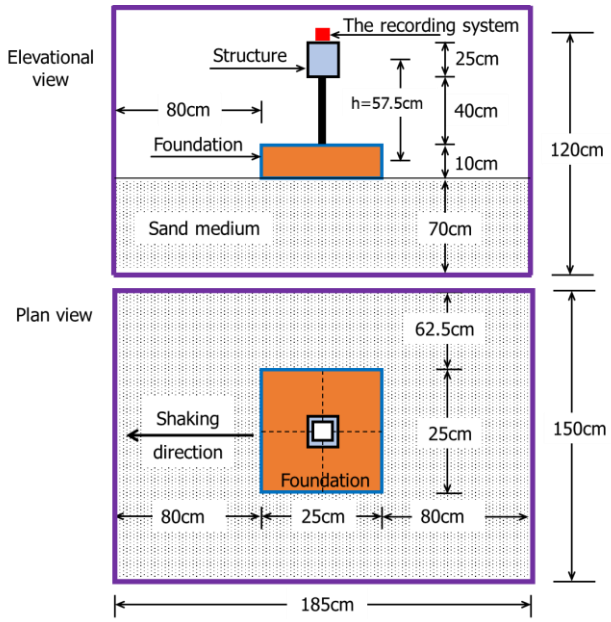

Fig. 4 Dimensional characteristics of the footing and the soil container

Vietnam to study a simplified structure lying on sand with a known density.

With 2 m×2 m dimensions of R202(UTC) shaking table; the final length, width, depth, and thick of the rigid soil container have been selected to be 1.85m, 1.5m, 1.2m, and 10 mm, respectively. The test model with three main components is located at the center of the fill surface. This model consists of three main structural components: a 0.25 m sided square shallow foundation block at the bottom, a steel mass with 150kg at top and a 0.4m of HEB steel beam connecting two massive blocks. The effective height of the model is $h = \frac{0.1}{2} + 0.4 + \frac{0.25}{2} = 0.575m$ (see Fig. 4 and 5). The recording system consists of an accelerometer and a displacement sensor placed on the top of the model.

The dry sand was filled in the container and compacted in layers with relative density $D_r = 82\%$, mass density $\rho = 1.66\ g/cm^3$, angle of internal friction $\varphi = 42.6^o$ and 0.7m high. The ultimate bearing capacity under vertical central load defined by Terzaghi's formula.

$$N_{max} = Sq_{max} = (B \times B)q_{max} \quad (16)$$

$$q_{max} = 1.3c'N_c + qN_q + 0.4\gamma BN_\gamma \quad (17)$$

c'=0; q= γD_f=0; $\gamma = 1.66\frac{g}{cm^3} \times \frac{9.81m}{s^2} = 16.29\frac{kN}{m^2}$; $N_\gamma = 171.99$. Hence, $N_{max} = (0.25 \cdot 0.25) \cdot (0.4 * 0.25 \cdot 16.29 \cdot 171.99) = 17.51kN$. Total weight of the specimen is $N = (m_0 + m_{col} + m_1) \times g = (15 + 6.88 + 150) \cdot 9.81 \cdot 10^{-3} = 1.69kN$. The static safety factor is $F_S = N_{max}/N = 17.51/1.69 = 10.36$ in range from 9 to 24 (Paolucci *et al.* 2008).

The shaking table was excited by the long-duration acceleration history (see Fig. 6) of Tolmezzo Earthquake. Five earthquake motions are denoted from N1 to N5 corresponding maximum acceleration to 0.1 m/s^2, 0.2 m/s^2, 0.4 m/s^2, 0.8 m/s^2 and 1.4 m/s^2.

Fig. 5 The test model in the soil container

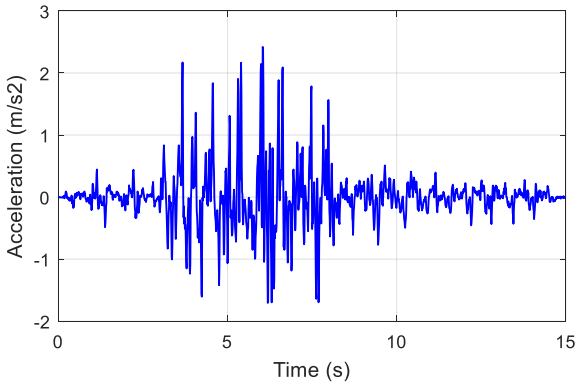

Fig. 6 Tolmezzo earthquake acceleration

Table 1 Parameters of the numerical model

k_x (N/m)	k_{ry} (Nm/rad)	k_z (N/m)	k_{1x} (N/m)	c_x (Ns/m)	c_{ry} (Ns/m)	c_z (Ns/m)
$202.68 \cdot 10^6$	$201.74 \cdot 10^5$	$338.48 \cdot 10^6$	$120.88 \cdot 10^5$	$1.34 \cdot 10^5$	$1.26 \cdot 10^3$	$2.42 \cdot 10^5$
c_{1x} (Ns/m)	m_1 (kg)	m_0 (kg)	h (m)	J (kg m^2)	N_{max} (kN)	$\mu = \frac{3}{4}tan\varphi$
0	150	15	0.575	50.12	17.51	0.69
ψ	ξ	λ	χ	δ_1	δ_2 (1/rad)	
0.43	0.95	4	6	0.75	5000	

3.2 Comparison of simulation and experimental results

In the macro-element model, five lateral motions were also applied to the soil-structure system in chronological order. Linear behaviour of the superstructure is assumed. The values of dynamic impedances of soil in the elastic range, the stiffness of the steel column, the masses and other parameters obtained from the respective sample test are given in Table 1.

Figs. 7-9 shows the comparison of the acceleration and the displacement at the top of structure for N3 and N4. As can be seen, the simulation was reproduced the experimental results.

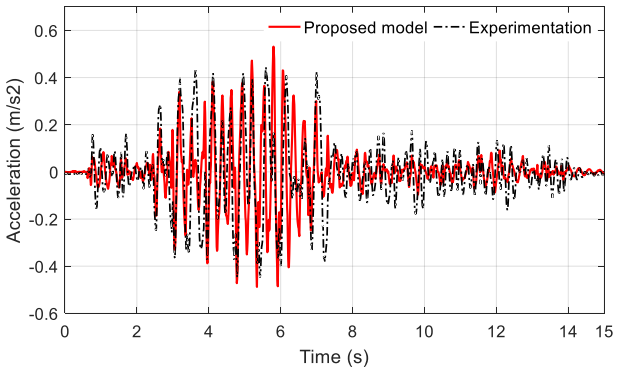

Fig. 7 Test N4- the acceleration of the top of structure

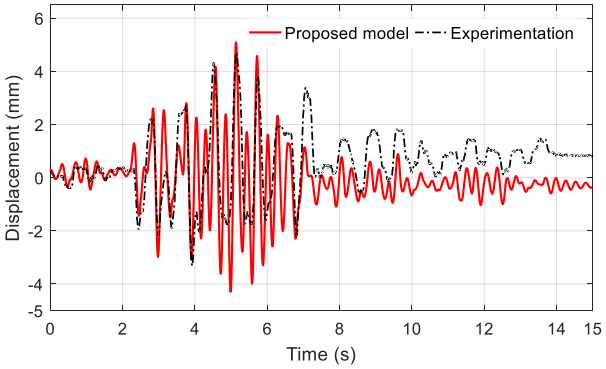

Fig. 8 Test N3- the displacement of the structure

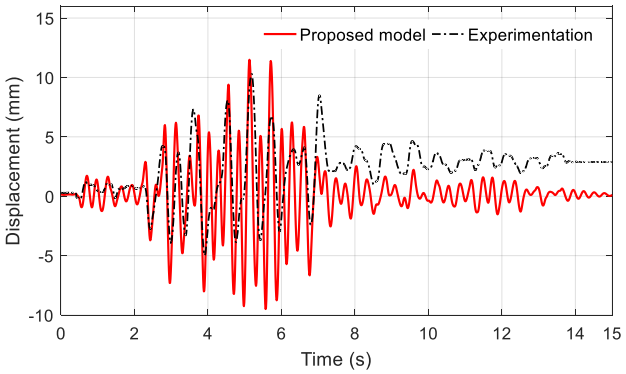

Fig. 9 Test N4- the displacement of the structure

However, the responses of structure can't match with the experimental results for the final test N5 (Fig. 10, 11). This difference probably comes from the fact that the accelerations which are applied in chronological order from test N1 to test N5 during the experiment would result in the accumulated effect on the structure. In contrary, the simulation tests have been launched independently. It makes the simulation results are quite different with the experimental result at the last test. It is also notable that Fig. 10 and Fig. 11 represent only the results during the first five seconds of test N5 because the structure has been overturned from the fifth second of test N5.

Table 2 represents the maximum values of the acceleration and the displacement at top of superstructure obtained from test N1 to test N5. These maximum values correspond to the time of 6.5s, 5.4s, 4.4s for test N3, test N4

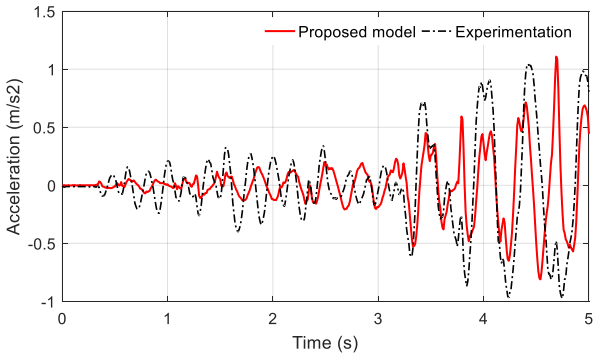

Fig. 10 Test N5- the acceleration of the structure

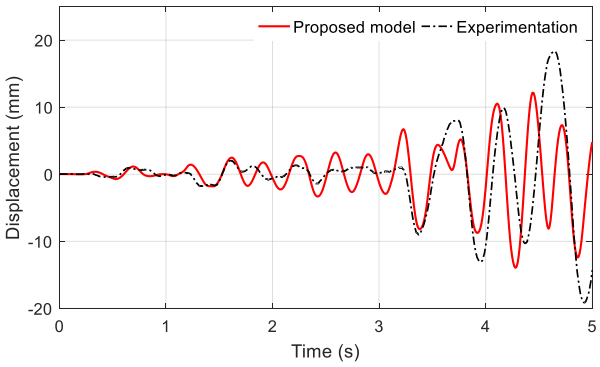

Fig. 11 Test N5- the displacement of the structure

Table 2 Maximum values of acceleration and displacement at top of superstructure

Test	Acceleration			Displacement		
	Experimentation (m/s^2)	Macro-element (m/s^2)	Error (%)	Experimentation (mm)	Macro-element (mm)	Error (%)
N1	0.155	0.149	4.03	0.616	0.582	5.84
N2	0.222	0.232	4.31	1.336	1.229	8.71
N3	0.357	0.373	4.29	4.707	5.065	7.07
N4	0.457	0.531	13.97	10.31	11.470	10.11
N5	1.045	1.109	5.77	Overturned	-	-

and test N5, respectively. It's found that the responses of structure where soil-foundation system simulated by the macro-element are suitable to experimentations.

3.3 Effect of the stiffness K^S

In Paolucci's model, the differential motion form of Newmark time integration was represented by Eq. (18):

$$\begin{aligned}\left[\frac{\boldsymbol{M}}{\beta(\Delta t)^2}+\frac{\boldsymbol{C}\gamma}{\beta\Delta t}\right]\boldsymbol{x}_{n+1}+\boldsymbol{F}_{n+1}(\boldsymbol{x}_{n+1}) &= \boldsymbol{P}_{n+1} \\ &+\boldsymbol{M}\left[\frac{1-2\beta}{2\beta}\ddot{\boldsymbol{x}}_n+\frac{\dot{\boldsymbol{x}}_n\Delta t+\boldsymbol{x}_n}{\beta(\Delta t)^2}\right] \\ &+\boldsymbol{C}\left[\left(\frac{\gamma}{2\beta}-1\right)\ddot{\boldsymbol{x}}_n\Delta t+\left(\frac{\gamma}{\beta}-1\right)\dot{\boldsymbol{x}}_n\right. \\ &\left.+\frac{\gamma}{\beta\Delta t}\boldsymbol{x}_n\right]\end{aligned} \quad (18)$$

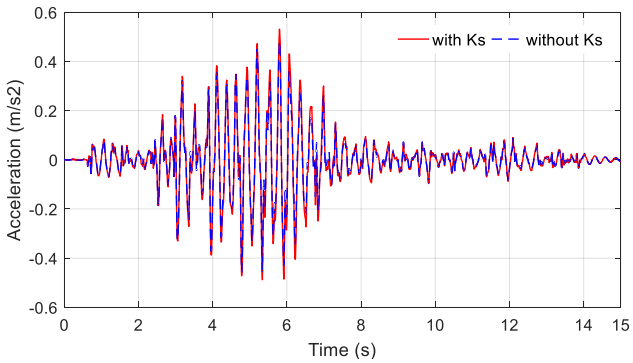

Fig. 12 Test N4-the effect of $\boldsymbol{K}^S$ to the acceleration at the top of structure

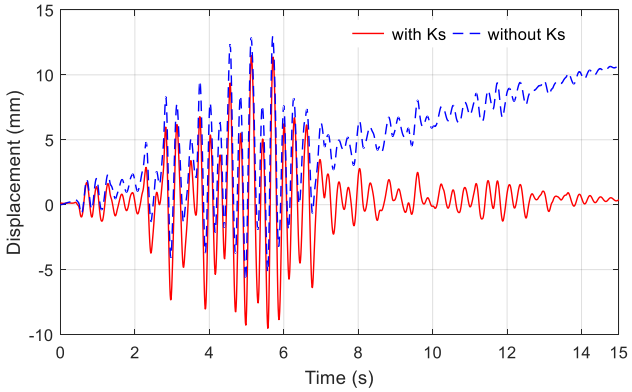

Fig. 13 Test N4-the effect of $\boldsymbol{K}^S$ to the displacement at the top of superstructure

It is noted that the stiffness $\boldsymbol{K}^S$ have been neglected in this equation. We have corrected it in the proposed model by adding $\boldsymbol{K}^S$ as mentioned in Chopra (1995) (see Eq. (8)). Fig. 12 shows the comparison between the proposed model (with $\boldsymbol{K}^S$) and the Paolucci's model (without $\boldsymbol{K}^S$) in term of acceleration at the top of structure. It is found that two curves are generally close.

However, it was observed a difference between the two models in term of displacement at the top of structure (Fig. 13). It might result from the negligence of $\boldsymbol{K}^S$ in the differential motion form of Newmark time integration. When $\boldsymbol{K}^S$ was mentioned in the proposed model, the curve matched better with the experimental results (see Fig. 9).

4. Conclusions

In this paper, a macro-element for modelling the behavior of SSI under seismic loading have been represented. The proposed macro-element consists of 4 DOFs in which the superstructure is lumped as a single DOF and the system of soil-foundation is modelled by 3 DOFs. It considered simultaneously the effect of material and geometric nonlinearities on the response of soil-structure interaction. As demonstrated by the results presented herein, the model was able to reproduce the response of SSI under seismic loading. The effect of the stiffness $\boldsymbol{K}^S$ in the differential motion form of Newmark time integration was also analyzed. It found that in term of acceleration, the result from macro-element wasn't much different in comparison with the experimental results. However, by negligence of the stiffness $\boldsymbol{K}^S$, the simulated results in term of displacement at the top of structure can't match with the experimental results.

Acknowledgments

The research presented in this paper was financially supported by University of Transport and Communications, Vietnam, through Grant number T2020-PHII-005.

References

Anastasopoulos, I., Kourkoulis, R., Gelagoti, F. and Papadopoulos, E. (2012), "Rocking response of sdof systems on shallow improved sand: An experimental study", *Soil Dyn. Earthq. Eng.*, **40**, 15-33. https://doi.org/10.1016/j.soildyn.2012.04.006.

Chai, S., Ghaemmaghami, A.R. and Kwon, O. (2017), "Numerical modelling method for inelastic and frequency-dependent behavior of shallow foundations", *Soil Dyn. Earthq. Eng.*, **92**, 377–387. https://doi.org/10.1016/j.soildyn.2016.10.030.

Chatzigogos, C.T., Figini, R., Pecker, A. and Salençon, J. (2011), "A macroelement formulation for shallow foundations on cohesive and frictional soils", *Int. J. Numer. Anal. Meth. Geomech*, **35**(8), 902-931. https://doi.org/10.1002/nag.934.

Chatzigogos, C.T., Pecker, A. and Salencon, J. (2009), "Macroelement modeling of shallow foundations", *Soil Dyn. Earthq. Eng.*, **29**(05), 765–781. https://doi.org/10.1016/j.soildyn.2008.08.009.

Chopra, A.K. (1995), *Dynamics of Structures*, Pearson, London, U.K.

Cremer, C., Pecker, A. and Davenne, L. (2001), "Cyclic macro-element for soil-structure interaction: material and geometrical non-linearities", *Int. J. Numer. Anal. Meth. Geomech.*, **25**(13), 1257-1284. https://doi.org/10.1002/nag.175.

Cremer, C., Pecker, A. and Davenne, L. (2002), "Modelling of nonlinear dynamic behavior of a shallow strip foundation with macro-element", *J. Earthq. Eng.*, **06**(02), 175-211. https://doi.org/10.1080/13632460209350414.

Di Prisco, C. and Pisano, F. (2011), "Seismic response of rigid shallow footings", *Eur. J. Environ. Civ. Eng.*, **15**(1), 185-221. https://doi.org/10.1080/19648189.2011.9695308.

Figini, R., Paolucci, R. and Chatzigogos, C.T. (2012), "A macro-element model for non-linear soil–shallow foundation–structure interaction under seismic loads: theoretical development and experimental validation on large scale tests", *Earthq. Eng. Struct. Dyn*, **41**(03), 475-493. https://doi.org/10.1002/eqe.1140.

Gazetas, G. (1991), *Foundation Vibrations in Foundation Engineering Handbook*, Chapter 15, Springer, Boston, Massachusetts, U.S.A.

Grange, S., Kotronis, P. and Mazars, J. (2008), "A macro-element for a circular foundation to simulate 3d soil–structure interaction", *Int. J. Numer. Anal. Meth. Geomech,* **32**(10), 1205-1227. https://doi.org/10.1002/nag.664.

Grange, S., Kotronis, P. and Mazars, J. (2009), "A macro-element to simulate dynamic soil-structure interaction", *Eng. Struct.*, **31**(12), 3034-3046. https://doi.org/10.1016/j.engstruct.2009.08.007.

Huynh, V.Q., Nguyen, X.H. and Nguyen, T.K. (2020), "A macro-element for modelling the non-linear interaction of soil-shallow

foundation under seismic loading", *Civ. Eng. J.*, **6**(4), 714-723. https://doi.org/10.28991/cej-2020-03091503.

Khebizi, M., Guenfoud, H. and Guenfoud, M. (2018), "Numerical modelling of soil-foundation interaction by a new non-linear macro-element", *Geomech. Eng.*, **14**(4), 377-386. https://doi.org/10.12989/gae.2018.14.4.377.

Millen, M.D.L., Cubrinovski, M., Pampanin, S. and Carr, A. (2018), "A macro-element for the modelling of shallow foundation deformations under seismic load", *Soil Dyn. Earthq. Eng.*, **106**, 101-112. https://doi.org/10.1016/j.soildyn.2017.12.001.

Nova, R. and Montrasio, L. (1991), "Settlements of shallow foundations on sand", *Geotechnique*, **41**(2), 243-256. https://doi.org/10.1680/geot.1991.41.2.243.

Page, A.M, Grimstad, G., Eiksund, G.R. and Jostad, H.P. (2018), "A macro-element pile foundation model for integrated analyses of monopilebased offshore wind turbines", *Ocean Eng.,* **167**, 23-35. https://doi.org/10.1016/j.oceaneng.2018.08.019.

Page, A.M, Grimstad, G., Eiksund, G.R. and Jostad, H.P. (2019), "A macro-element model for multidirectional cyclic lateral loading of monopiles in clay", *Comput. Geotech.*, **106**, 314-326. https://doi.org/10.1016/j.compgeo.2018.11.007.

Paolucci, R. (1997), "Simplified evaluation of earthquake-induced permanent displacements of shallow foundations", *J. Earthq. Eng.*, **1**(3), 563-579. https://doi.org/10.1080/13632469708962378.

Paolucci, R., Shirato, M. and Yilmaz, M.T. (2008), "Seismic behavior of shallow foundations: shaking table experiments vs numerical modelling", *Earthq. Eng. Struct. Dyn*, **37**(4), 577-595. https://doi.org/10.1002/eqe.773.

Pecker, A., Paolucci, R., Chatzigogos, C., Correia, A.A. and Figini, R. (2014), "The role of non-linear dynamic soil-foundation interaction on the seismic response of structures", *Bull. Earthq. Eng.*, **12**, 1157-1176. https://doi.org/10.1007/s10518-013-9457-0.

Salciarinia, D., Frizzaa, M., Tamagninia, C., Arroyob, M. and Abadìas, D. (2016), "Macroelement modeling of SSI effects on offshore wind turbines subject to large number of loading cycles", *Procedia Eng.*, **158**, 332-337. https://doi.org/10.1016/j.proeng.2016.08.451.

Tistel, J., Grimstad, G. and Eiksund, GR. (2020), "A macro model for shallow foundations on granular soils describing nonlinear foundation behaviour", *Comput. Struct.,* **232**, 105816. https://doi.org/10.1016/j.compstruc.2017.07.018.

Venanzi, I., Salciarini, D. and Tamagnini, C. (2014), "The effect of soil-foundation-structure interaction on the wind-induced response of tall buildings", *Eng. Struct.,* **79**, 117-130. https://doi.org/10.1016/j.engstruct.2014.08.002.